F. Malone
GMedTech,
Department of Mechanical and
Industrial Engineering,
Galway-Mayo Institute of Technology,
Galway H91 T8NW, Ireland
e-mail: fiona.malone@gmit.ie

E. McCarthy
GMedTech,
Department of Mechanical and
Industrial Engineering,
Galway-Mayo Institute of Technology,
Galway H91 T8NW, Ireland

P. Delassus
GMedTech,
Department of Mechanical and
Industrial Engineering,
Galway-Mayo Institute of Technology,
Galway H91 T8NW, Ireland

J. H. Buhk
Department of Diagnostic and
Interventional Neuroradiology,
University Medical Center Hamburg-Eppendorf,
Martinistr. 52,
Hamburg 20246, Germany

J. Fiehler
Department of Diagnostic and
Interventional Neuroradiology,
University Medical Center Hamburg-Eppendorf,
Martinistr. 52,
Hamburg 20246, Germany

L. Morris
GMedTech,
Department of Mechanical and
Industrial Engineering,
Galway-Mayo Institute of Technology,
Galway H91 T8NW, Ireland
e-mail: liam.morris@gmit.ie

Embolus Analog Trajectory Paths Under Physiological Flowrates Through Patient-Specific Aortic Arch Models

Atrial fibrillation (AF) is the most common irregular heartbeat among the world's population and is a major contributor to cardiogenic embolisms and acute ischemic stroke (AIS). However, the role AF flow plays in the trajectory paths of cardiogenic emboli has not been experimentally investigated. A physiological simulation system was designed to analyze the trajectory patterns of bovine embolus analogs (EAs) ($n = 720$) through four patient-specific models, under three flow conditions: steady flow, normal pulsatile flow, and AF pulsatile flow. It was seen that EA trajectory paths were proportional to the percentage flowrate split of 25–31% along the branching vessels. Overall, AF flow conditions increased trajectories through the left- (LCCA) and right (RCCA)-common carotid artery by 25% with respect to normal pulsatile flow. There was no statistical difference in the distribution of clot trajectories when the clot was released from the right, left, or anterior positions. Significantly, more EAs traveled through the brachiocephalic trunk (BCT) than through the LCCA or the left subclavian. Yet of the EAs that traveled through the common carotid arteries, there was a greater affiliation toward the LCCA compared to the RCCA ($p < 0.05$). [DOI: 10.1115/1.4043832]

Keywords: atrial fibrillation, acute ischemic stroke, physiological simulation, cardiogenic emboli, aortic arch

1 Introduction

Acute ischemic stroke (AIS) results from the sudden occlusion of a major cerebral artery [1]. Cardiogenic embolisms account for approximately 15% of AIS cases worldwide [2,3]. When a cardiac source embolus enters the cardiovascular system, it first must travel along the ascending aorta and may travel along the aortic arch and down the descending aorta or it may travel through the various vessels branching off the aortic arch (Fig. 1(*a*)). If the embolus enters the carotid arteries, it can become lodged within the smaller vessels of the cerebral vasculature, thus causing a stroke.

Atrial fibrillation (AF) is the most significant contributor to thrombus formation within the heart and is responsible for 45% of all cardio-embolic strokes [4]. During AF, blood pools in the left atrium resulting in clot formation within the heart. Approximately 90% of thrombi formed by AF are caused by the presence of a left atrial appendage [5,6]. This risk increases with age, where AF is the direct cause of 1 in 4 strokes in patients >80 yr old [7–9].

Blood clot trajectories have previously been modeled computationally [10–21] and experimentally [20–27]. Choi et al. [10] numerically assessed the trajectories of rigid, spherical particles within an idealized three-dimensional aortic arch model, comprising three branching arteries under AF conditions. Chung et al. [23] injected polyamide micro particles of 200, 500, and 1000 μm into commercially available CoW models. Others have analyzed trajectories through isolated bifurcations [22,27]. Fahy et al. (2015) fabricated thrombus analogs of 3 mm diameter, from crustacean hemolymph and tracked the clot trajectories within a thin-walled circle of Willis (CoW) phantom and assessed the hemodynamic effects and clot lodgment preferences. Clark et al. [26] developed a steady flow in vitro benchtop model of cerebral thromboembolism. To the best of the author's knowledge, there is currently no in vitro test system that experimentally releases mammalian blood clot analogs, through patient-specific aortic

Manuscript received April 9, 2018; final manuscript received May 13, 2019; published online July 15, 2019. Assoc. Editor: C. Alberto Figueroa.

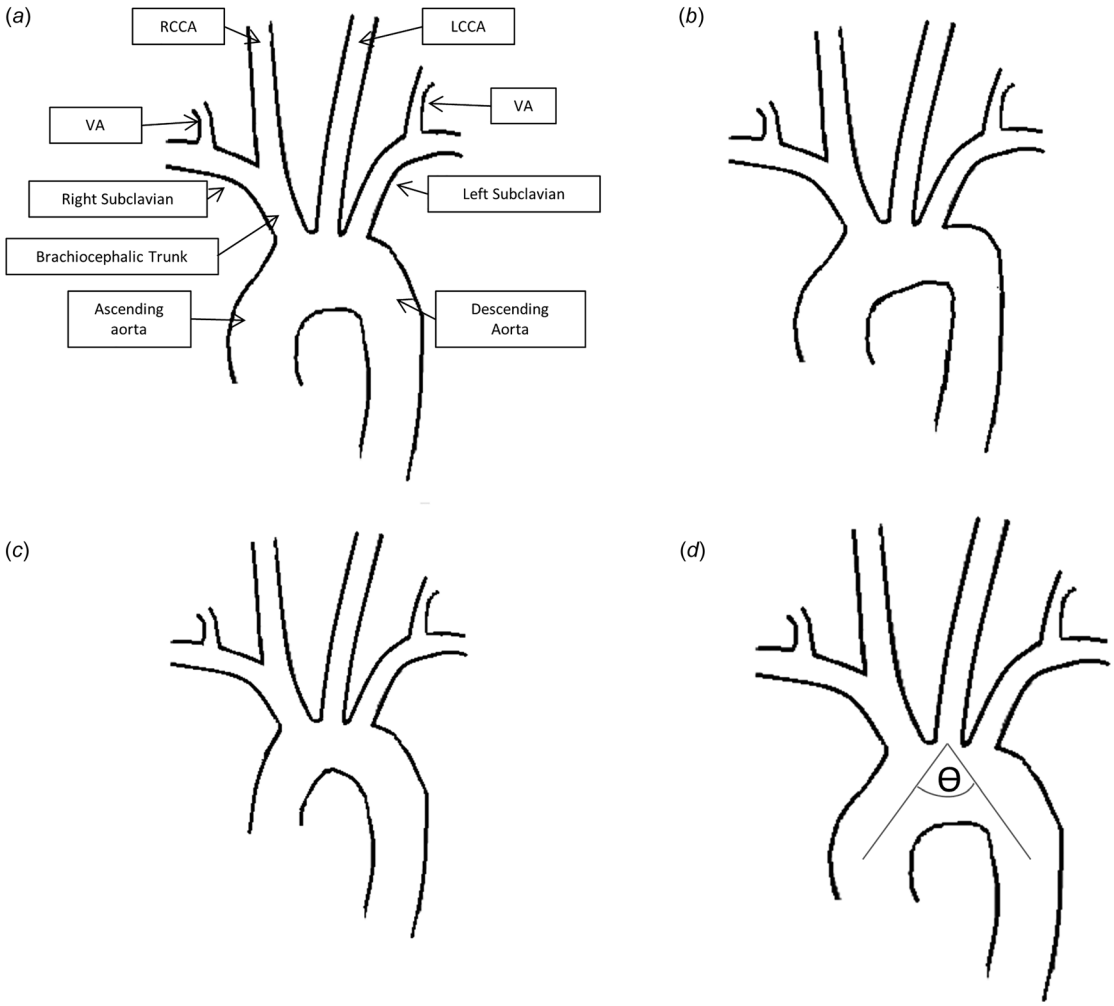

Fig. 1 (*a*) Schematic of a Romanesque aortic arch with branch labeling, (*b*) crenel aortic arch, (*c*) gothic aortic arch, and (*d*) aortic arch angulation, as described by Ou et al

arch cases, incorporating the branching vessels off the aortic arch leading to the arms and cranial vasculature. This study experimentally assessed the trajectory patterns of cardiogenic emboli under various flow conditions along four AF patient-specific aortic arch configurations. The hypothesis for this study is that EA trajectories along branching vessels are distributed proportionally to aortic arch configurations, flow types, and along each branching vessel. These tests will provide a unique insight into cardiogenic emboli and the chances a clot traveling to the cerebral vasculature will cause a stroke.

2 Materials and Methods

2.1 Aortic Arch Replication. Four aortic arch image data sets in digital imaging and communications in medicine format were obtained from the University Medical Center Hamburg-Eppendorf (UKE), Germany. Three of these cases were AF patients (models 1–3), who suffered a stroke (Table 1). Each model contained the ascending and descending aorta, the brachiocephalic trunk (BCT), right common carotid artery (RCCA), left common carotid artery (LCCA), and left and right subclavian arteries and vertebral arteries (VAs). Table 1 displays the arch geometry, type, branching variation, and vessel dimensions, as well as patient age and occlusion location. The four arches displayed all three major aortic arch geometries as described by Uflacker: Romanesque ($n = 2$, models 1 and 2, Fig. 1(*a*)), Crenel ($n = 1$, model 3, Fig. 1(*b*)), and Gothic ($n = 1$, model 4, Fig. 1(*c*)) [28]. The Romanesque arch shape is the most common among the global population (80%) and resembles a normal rounded aortic arch compared to the less common Crenel and Gothic shapes [28,29]. The aortic arch shape can also be described by the aortic arch angle (Θ, Fig. 1(*d*)), defined as the angle between a line connecting the highest point of the aortic arch and the midluminar point of the ascending and descending aorta [29,30]. Three types of aortic arch patterns have been previously described, with type I aortic arch the most common [31].

The commercially available, reconstruction software, MIMICS (Materialise, Leuven, Belgium) was used to generate the three-dimensional (3D) geometries from the two-dimensional medical image data sets (Figs. 2(*a*), 2(*c*), 2(*e*), and 2(*g*)) by applying various segmentation and smoothing methods as previously described by Fahy et al. [24], generating rigid hollow models saved in stereolithography format. Models 1, 2, and 4 all displayed a normal three-branch pattern off the aortic arch, while model 3 was a two-branching pattern, comprising of a common origin of the BCT and LCCA, with the left subclavian artery referred to as a bovine arch. The selected stroke cases had a range of occlusion types all occurring on the right side. These occlusions occurred within the internal carotid artery (ICA) ($n = 1$) and M1 ($n = 2$). The hollow models were 3D printed in Watershed stereolithography material (LPE 3D printing, Belfast, UK). Figures 2(*b*), 2(*d*), 2(*f*), and 2(*h*) display the printed models 1–4, respectively, fixated within the physiological simulation system.

2.2 Physiological Flow Replication. A blood mimicking fluid mixture of glycerin and water in a ratio of 40:60 by weight

Table 1 Patient and geometrical summary of the medial image dataset

Model number	Arch	Branching type	Branching variation	Age (yr)	Aortic arch angulation (deg)	Type of occlusion	Diameter (mm)					
							Aortic Arch D)	BCT	R Sub	RCCA	LCCA	L Sub
1	Romanesque	II	Trunk, LCCA, L Sub	77	96	Distal M1 right	27.27 ± 2.622	14.64 ± 0.520	11.17 ± 2.624	8.01 ± 0.379	7.63 ± 0.916	10.49 ± 0.734
2	Romanesque	I	Trunk, LCCA, L Sub	74	81	M1 right	29.31 ± 4.323	14.87 ± 1.045	9.35 ± 2.140	7.18 ± 0.875	7.96 ± 0.701	12.13 ± 4.170
3	Crenel	II	Common origin of trunk and LCCA, L Sub	77	73	Distal ICA right	28.74 ± 1.767	13.71 ± 3.228	12.74 ± 4.204	7.34 ± 0.306	9.88 ± 0.634	9.35 ± 0.744
4	Gothic	III	Trunk, LCCA, L Sub	85	70	N/A	26.85 ± 3.201	12.48 ± 0.576	7.34 ± 1.861	6.21 ± 0.596	6.30 ± 0.782	5.83 ± 0.717

Fig. 2 (*a*) and (*b*) Model 1, (*c*) and (*d*) model 2, (*e*) and (*f*) model 3, (*g*) and (*h*) model 4 (*a*, *c*, *e*, *g*: models created using mimics; *b*, *d*, *f*, *h*: 3D printed aortic arches)

with a viscosity of 3.7 mPa·s as tested in a viscometer (Brookfield DV-II+Pro, Middleboro, MA) and a density of 1058.33 kg m^{-3} at 21.1 °C was pumped through the models in a closed-loop system at room temperature. One steady and two pulsatile (normal and AF) flow conditions were simulated. The steady flow circuit was set up using a direct drive pump (RD-05HV24, Iwaki Direct Drive Pump, Tokyo, Japan) generating a cardiac output of 5 Lmin-1. A linear actuator (Aerotech, UK) controlled a piston pump, which replicated the pulsatile waveforms. The replication of normal ascending aorta blood flow was based upon previously published data [32] (Fig. 3(*a*)). The cardiac output and pulse period of the normal flowrate were reduced by 30 and 40%, respectively, to recreate the AF flow conditions (Fig. 3(*a*)). A similar scaling factor was applied by Choi et al. [10] for their numerical analysis, which was based on the clinical observations of normal sinus rhythm and AF cardiac output conditions [33]. Figures 3(*b*) and 3(*c*) display the measured inlet flow rates for all cases. These replicated flowrates showed good agreement with the flowrates. These cardiac outputs were within the reported range [34]. Table 2 displays the average inlet and outlet flow rates measured using an ultrasonic flow meters (25 PXL flowsensor, Transonic,

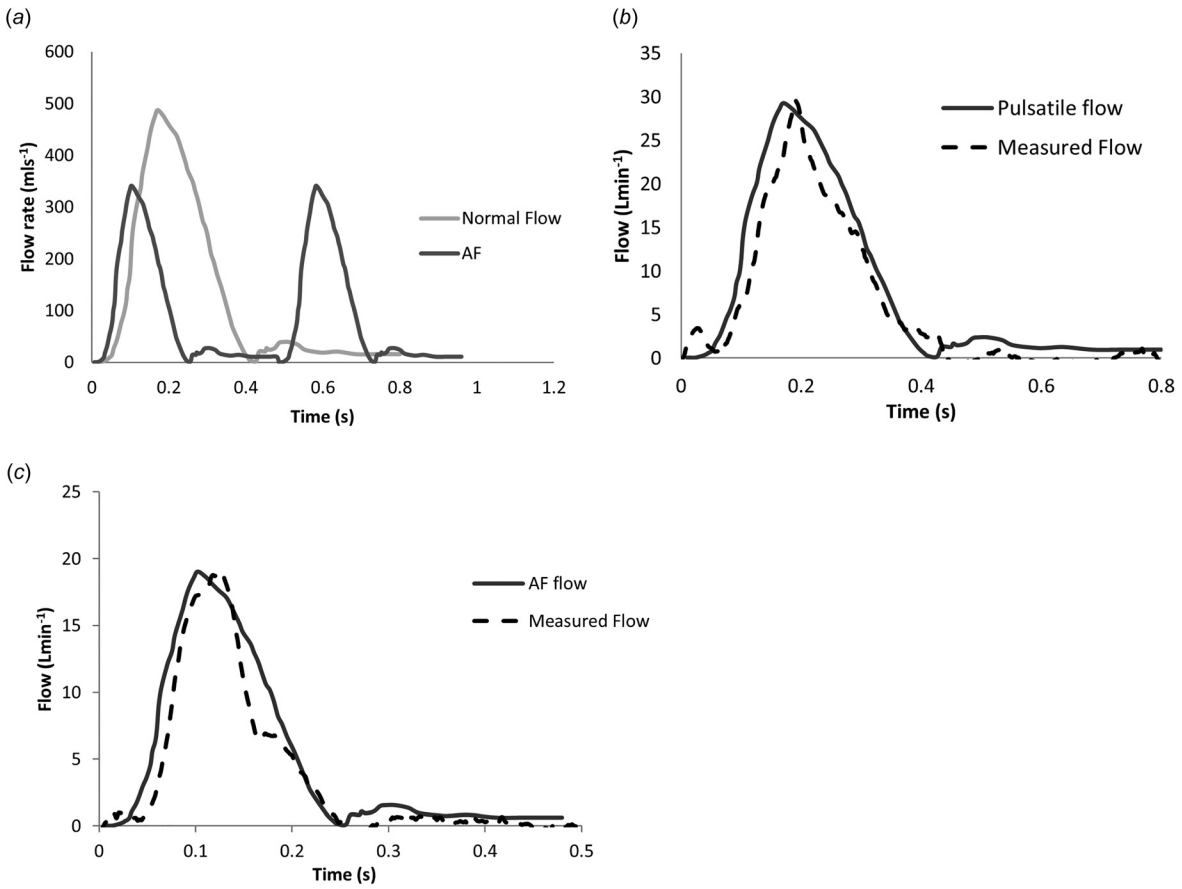

Fig. 3 (*a*) Normal and AF pulsatile flowrate profiles, (*b*) healthy measured flow, and (*c*) AF measured flow

Table 2 Average flow rates along each vessel for the four aortic arch models under three different flow conditions: steady, normal, and AF

Artery	Average steady flow (ml min^{-1})	Average normal flow (ml min^{-1})	Average AF flow (ml min^{-1})
Ascending aorta	5450 ± 173.21	7150 ± 57.74	4925 ± 192.03
Right subclavian	350 ± 57.74	550 ± 50.00	395 ± 8.66
RCCA	350 ± 57.74	375 ± 43.30	295 ± 8.66
BCT	700 ± 81.65	925 ± 43.30	700 ± 0.00
LCCA	350 ± 57.74	375 ± 43.30	288 ± 21.65
VAs	72.5 ± 22.17	95 ± 8.66	85 ± 8.66
Left subclavian	400 ± 81.65	550 ± 50.00	375 ± 43.30
Descending aorta	3900 ± 57.74	5225 ± 82.92	3450 ± 165.83

Ithaca, NY). The same steady, normal, and AF waveforms were prescribed to the four aortic arch models.

Values from the literature were used to set the outlet flowrates. The flowrates along the right/left subclavian artery range from 360 ± 0.6 ml min^{-1} to 800 ml min^{-1} [35,36]. Blood flow to the brain can be up to 1000 ml min^{-1} [37] and Sato et al. reported blood flow values for the left and right common carotid arteries (363 ± 18 ml min^{-1}) and the vertebral arteries (90 ± 12 ml min^{-1}). The percentage outlet flow rate through the descending aorta varied from 69% to 75%, which is within the clinical range documented in literature [38,39].

Table 2 displays the average outlet flowrates measured for each of the seven outlet vessels. A 16PXL Clamp-on flowsensor (Transonic, Ithaca, NY) was utilized to measure and monitor the outlet flowrates. The geometry of the model played a major role in the splitting of the outlet flows. The flowrates were further controlled by valves to restrict flow through the outlets in order to maintain an average outlet flow rate representative of physiological outlet flow rates reported in literature. The control of the outlet flow split was extremely challenging to ensure each of the four models experienced the same outlet conditions. The outlet flow splits were balanced by trial and error and were continuously monitored and measured using the clamp on flowmeter before, during, and after each trajectory test to ensure each clot was subjected to the same flow conditions.

2.3 Embolus Analog Fabrication. Bovine blood was obtained from a local abattoir (Burkes, Gort, Galway, Ireland), which is an a European Union approved abattoir supervised by Galway County Council veterinary services. The blood was left to stagnate and coagulate (Fig. 4(*a*)). A previous study examined the mechanical properties of the bovine embolus analogs [40]. Briefly, the compression tests were executed by a 50 mm diameter plunger using an Instron 5544 (Instron 5500 series, Norwood, MA) on clots of height ranging from 15 to 20 mm and diameters

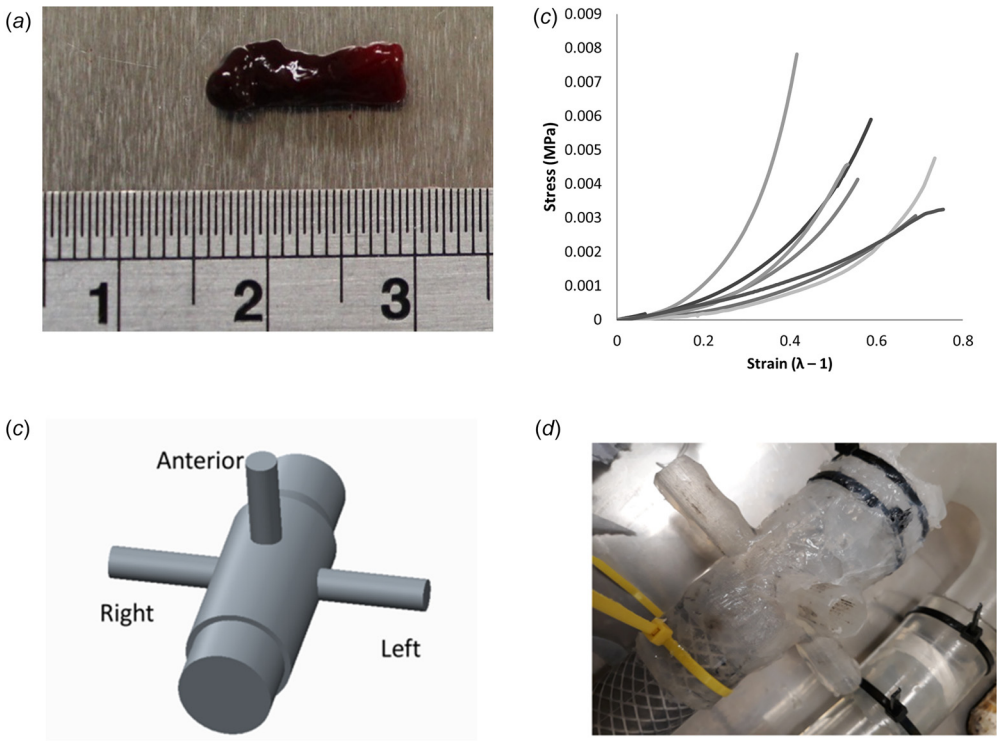

Fig. 4 (*a*) Sample of embolus analog prior to preparation, (*b*) compression testing results, (*c*) connector created for releasing clots, and (*d*) connector attached to model 1

of 30 mm at a rate of 0.25 mm/s. The embolus analogs displayed a compressive Young's modulus varying from 1.53 to 16.6 kPa for a percentage strain range of 5–40% (Fig. 4(*b*)), which was similar to other compressive studies found for human retrieved emboli [41]. The EAs fabricated for injection had an average diameter of 3.64 ± 0.76 mm and a length of 6.39 ± 1.81 mm as measured by an electronic digital caliper (Maplin, England) with an accuracy of 0.01 mm. These dimensions were similar to other EA sizes reported in literature [6,42].

A bespoke, flexible silicone connector was designed (Fig. 4(*c*)) and fabricated (Fig. 4(*d*)) for clot injection at the beginning of each cardiac cycle. Three inlet parts were positioned for injecting clots along the left, right, and anterior positions (Fig. 4(*c*)). The EA was placed within a tube and connected to the left, right, or anterior inlet. A syringe of the water–glycerin mixture was then inserted into the open end of the connecting tube and the fluid was injected to move the clot further into the connecting arm between two marker points. The valve was then closed and the clot remained stationary in the connector arm. Once the linear actuator was activated to start the cardiac cycle, clot entered into the arch.

2.4 Test Set Up. Figure 5(*a*) displays a schematic of the test setup and Fig. 5(*b*) shows a photograph of the physiological simulation system. The system comprised of a linear actuator that moved a piston pump connected with two check valves. One valve permitted fluid from a reservoir to enter the pump's cavity during the suction phase, while the other valve propelled the fluid during the ejection phase. The drive and control of the linear motor was provided by the Soloist CP30 controller (Aerotech, UK), connected to the computer through a serial port connection.

Twenty EAs were injected into the connector inlet at the three different entrance locations resulting in 60 EAs being injected into each of the four models. These 60 tests were repeated under three different flow conditions, resulting in a total of 720 clots released during testing. Two cameras (50 Hz frame rate, 12 MPixels) were used to monitor EA trajectories. Between embolus preparation, test setup, running of the test, and data acquisition, one trajectory test took approximately 5–10 min to complete successfully. After each release of an embolus, the vessel in which it traveled through was noted and recorded using the camera located above the aortic arch model. The camera above the aortic arch model recorded the trajectory.

The χ^2 test was used to test the hypotheses whether EA trajectories are distributed proportionally to aortic arch geometry, flow-rate type, and through each branching vessel. In all cases, the experimental data were compared to the null hypothesis (uniform distribution of EAs) using a simple χ^2 goodness-of-fit test within MINITAB 17.0 (Minitab, Inc., State College, PA).

3 Results

Table 3 displays the number of EAs traveling along the outlet for the four aortic arch cases under steady, normal, and AF flow conditions with corresponding clot entry location. Under steady flow, model 1 (Romanesque) displayed the most trajectories toward the head, through the LCCA and RCCA (10 clots), compared to models 2, 3, and 4. Model 1 had the least number of EA trajectories through the left and right subclavian arteries (2 EAs) compared to model 2 (6 EAs), and models 3 and 4 (7 EAs each). Model 3 (Crenel, 2 branch variation) was the only model in this study in which an EA traveled through the vertebral arteries (Fig. 5: steady flow, anterior). The steady flow results were used to discern the impact of pulsatile flow. There was an increase in clot trajectories through the branching vessels under healthy flow (70 clots) and AF flow (82 clots) when compared to steady flow (64). In terms of the clots that traveled through the common carotid artery (CCA) vessels, steady and AF flow displayed similar CCA trajectory counts for models 1–3.

Under normal pulsatile flow conditions, model 4 (Gothic) displayed the most clot trajectories through the LCCA and RCCA (11 clots). Model 1 (Romanesque) and model 3 (Crenel) both experienced a decrease in the number of clots through the CCAs under normal pulsatile flow when compared to steady flow.

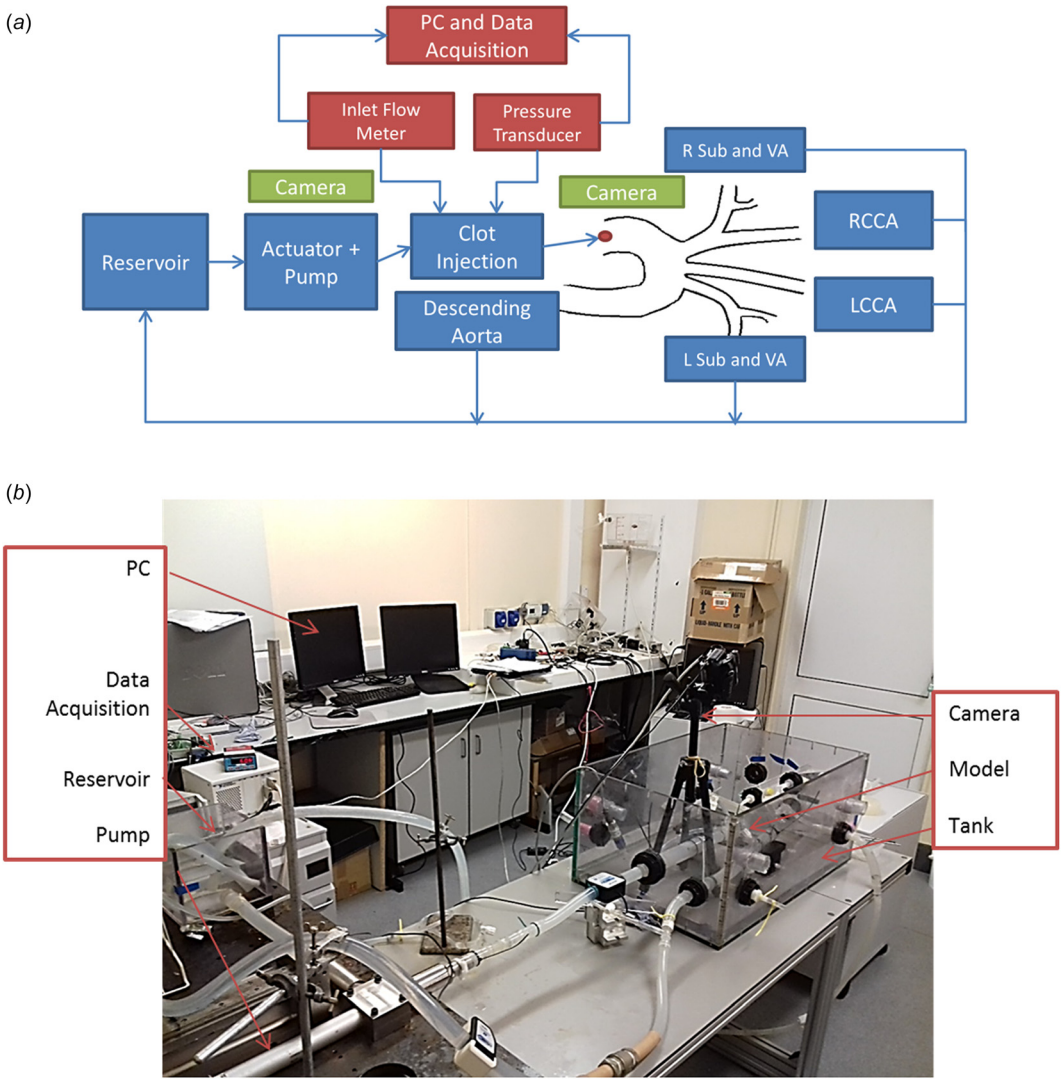

Fig. 5 (*a*) Schematic of experimental test setup and (*b*) picture of physiological simulation system

Table 3 Number of EAs traveling through outlet vessels under steady, normal, and AF flow conditions

		Steady				Normal				Atrial fibrillation			
Model	Vessel	Right	Anterior	Left	Total (%)	Right	Anterior	Left	Total (%)	Right	Anterior	Left	Total (%)
Model 1	LCCA	2	1	3	6 (10)	1	0	1	2 (3)	5	3	0	8 (13)
	RCCA	1	1	2	4 (7)	0	1	1	2 (3)	3	0	0	3 (5)
	Left sub	1	0	0	1 (2)	0	4	1	5 (8)	0	3	2	5 (8)
	Right sub	0	0	1	1 (2)	4	1	1	6 (10)	3	2	0	5 (8)
	Descending	16	18	13	48 (80)	15	14	16	45 (75)	9	12	18	39 (65)
Model 2	LCCA	0	3	1	4 (7)	1	2	2	5 (8)	3	3	0	6 (10)
	RCCA	0	1	1	2 (3)	0	1	0	1 (2)	0	0	1	1 (2)
	Left sub	1	1	1	3 (5)	4	2	1	6 (10)	0	0	1	1 (2)
	Right sub	3	0	0	3 (5)	2	1	2	6 (10)	1	0	4	5 (8)
	Descending	16	15	17	48 (80)	13	14	15	42 (70)	16	17	14	47 (78)
Model 3	LCCA	1	4	1	6 (10)	1	1	0	2 (3)	3	0	1	4 (7)
	RCCA	0	1	2	3 (5)	0	2	1	3 (5)	2	2	1	5 (8)
	Left sub	3	3	1	6 (10)	0	4	0	4 (7)	0	2	3	5 (8)
	Right sub	0	0	1	1 (2)	2	1	2	5 (8)	3	2	2	7 (12)
	Descending	16	12	15	43 (72)	17	12	17	46 (77)	12	14	13	39 (65)
Model 4	LCCA	4	1	1	6 (10)	3	2	3	8 (13)	2	4	3	9 (15)
	RCCA	0	0	0	0 (0)	0	2	1	3 (5)	0	0	1	1 (2)
	Left sub	0	0	3	3 (5)	2	2	0	4 (7)	3	4	2	9 (15)
	Right sub	3	1	0	4 (7)	2	2	4	8 (13)	3	2	3	8 (13)
	Descending	13	18	16	47 (78)	13	12	12	37 (62)	12	10	11	33 (55)

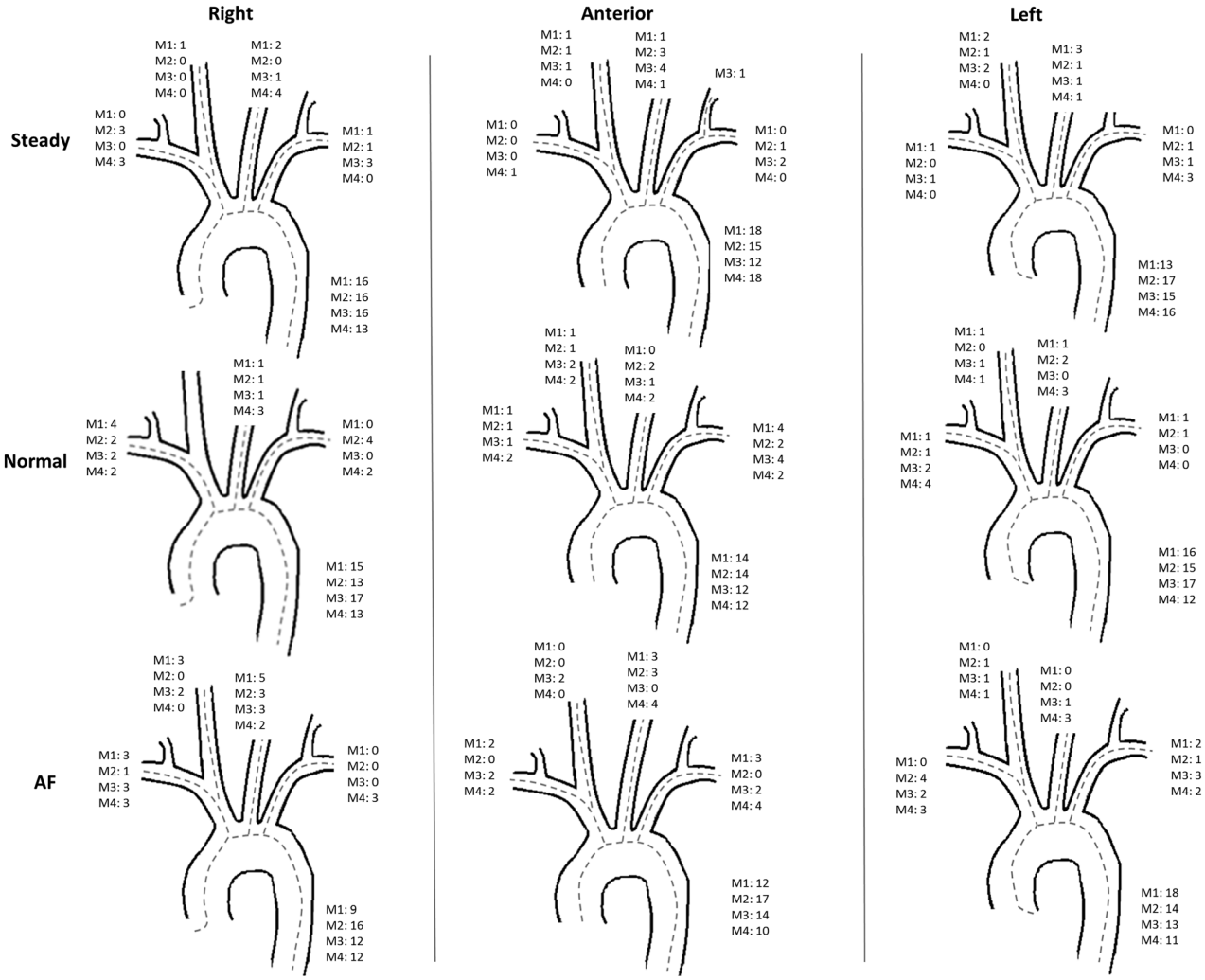

Fig. 6 Schematic of the clot trajectory paths through each model under three flow conditions. Each clot was released from the left, anterior, and right positions 20 times. The number of clots that took that trajectory path for each model is noted beside each output vessel.

The number of clots through the CCAs under steady and normal flow conditions through model 2 (Romanesque) was unchanged (6 clots). However, the number of clots that passed through the CCAs increased significantly in model 4 by 59%. Model 4 also had the largest number of clot trajectories through the subclavian arteries (12 EAs). This increase in the number of EAs traveling through the branching vessels off the aortic arch resulted in model 4 having the lowest number of EAs traveling through the descending aorta (37 EAs) compared to the other three models (>70%) for normal flow rates.

Under AF flow conditions, models 1, 2, and 3 all displayed an increase in clots paths through the CCAs when compared to clot trajectories under normal physiological flow. Model 1 experienced an increase of 150% in the number of cranial trajectories under AF flow (11 EAs) compared with those under normal physiological conditions (4 EAs). Models 1 and 2 (Romanesque) displayed a decrease in EA trajectories through the left and right subclavian arteries. Under AF flow conditions, models 3 (Crenel) and 4 (Gothic) both displayed a significant increase in the number of EAs that passed through the subclavian arteries compared to normal physiological flow conditions. The number of EAs traveling through the CCAs was similar for models 1, 2, and 3 under both AF and steady flow conditions.

Model 4 displayed the largest number of clots traveling toward the head across all three physiological flow conditions (27 clots). Model 4 also displayed the lowest number of clots traveling through the descending aorta (117 clots) compared to the other aortic arch models. Although the Gothic aortic arch geometry displayed a substantial increase in the number of EAs traveling through the CCA vessels, there was no statistical significance in the relationship between the four different models and clot trajectory patterns through the branching vessels and the descending aorta, $\chi^2\,(3, N = 720) = 5.90, p = 0.12$.

Figure 6 displays a schematic of the clot trajectory paths through each model and displays the number of blood clot trajectory paths through each model from the right, anterior, and left starting positions under steady, normal, and AF flow conditions. There was a statistical significance in the distribution of clot trajectories through the branching outlet vessels, with more clots traveling through the BCT, $\chi^2\,(2, N = 720) = 12.70, p < 0.05$.

Figure 7(*a*) displays the variation in the number of clots traveling through the brachiocephalic trunk, LCCA, and left subclavian under all three flow conditions across the four models. Figure 7(*b*) displays the variation in the number of clots traveling through the descending aorta under the three flow conditions across the four models. Figures 7(*c*) and 7(*d*) show an increase in clot trajectories though the aortic arch branches with AF flow, and a significant decrease in trajectories through the descending aorta, respectively, $\chi^2\,(2, N = 720) = 12.51, p < 0.05$.

The relationship between LCCA and RCCA trajectories was also significant, $\chi^2\,(3, N = 97) = 13.95, p < 0.05$. As can be seen from Figs. 8(*a*)–8(*c*), the LCCA was the more prominent of

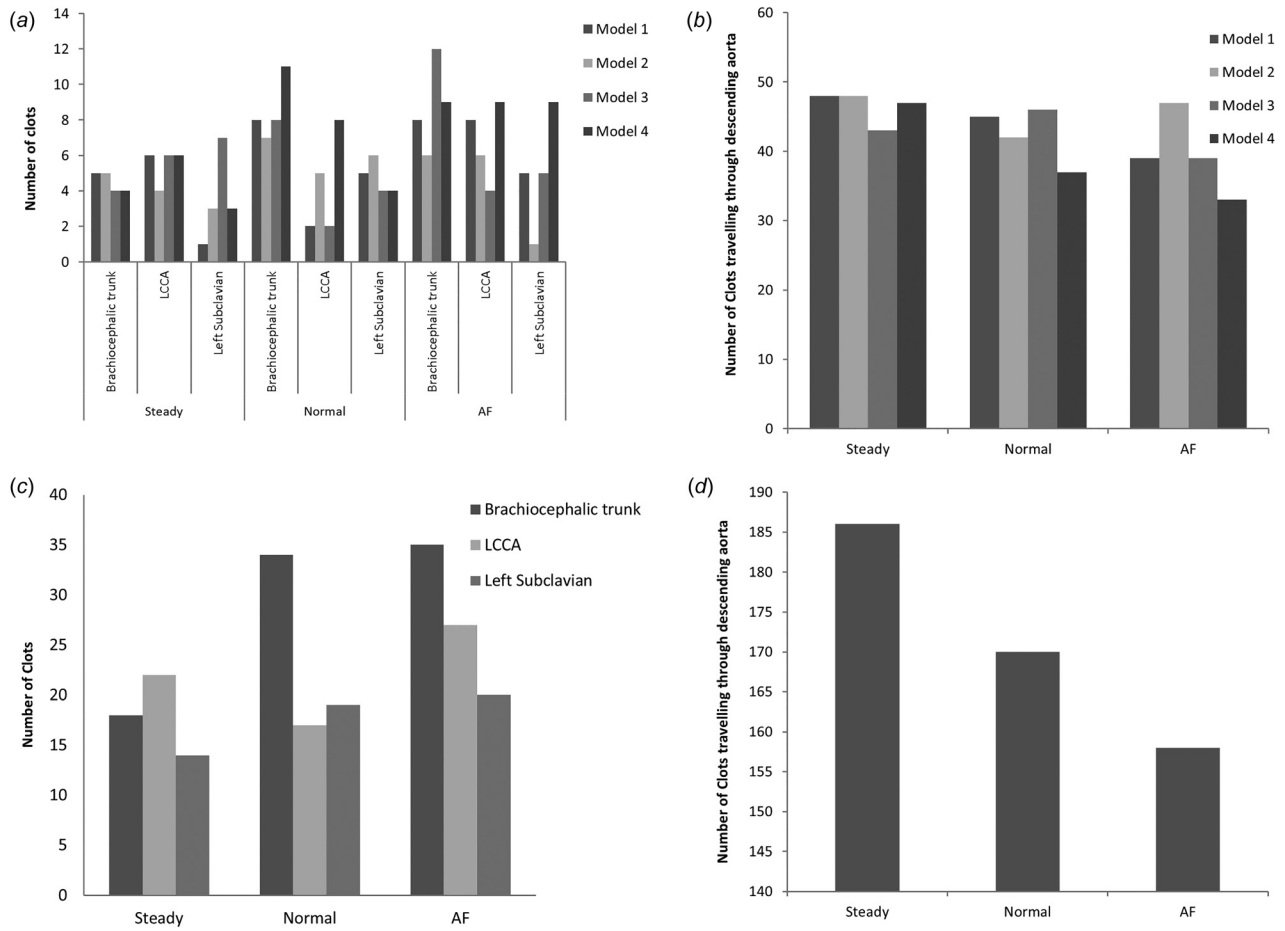

Fig. 7 (*a*) Bar chart of the variation in the number of clots traveling through the brachiocephalic trunk, LCCA, and left subclavian under the three flow conditions across the four models, (*b*) bar chart of the variation in the number of clots traveling through the descending aorta under the three flow conditions across the four models, (*c*) bar chart of the overall number of clots that traveled through the BCT, LCCA, and left subclavian under the three flow conditions, and (*d*) bar chart of the overall number of clots that traveled through the descending aorta

the two CCA vessels in terms of clot trajectory paths. Figure 8(*d*) shows a relatively equal distribution of EA trajectories through the left and right subclavian arteries.

4 Discussion

The purpose of this in vitro testing system was to investigate the role AF flow conditions may have on cardiogenic emboli trajectory paths using mammalian EAs and different aortic arch configurations. Few studies have simulated clot trajectories along the aortic arch with branching vessels. Clark et al. developed a steady flow in vitro bench top model of cerebral thromboembolism [26]. This model adapted an idealized arch geometry used by Osorio et al. [12] and used rigid, acrylic blood clot analogs of diameters 2, 3.5, and 5 mm. Fahy et al. [24] injected lobster EAs into a model of the internal carotid artery through a cerebral flow facility housing a manufactured phantom model of a patient-specific Circle of Willis model that did not include the aortic arch. Our system tested bovine EAs of known mechanical properties along four patient-specific aortic arches of varying geometry, angulation, and branching patterns under three flow conditions: steady, normal, and AF.

Two of the aortic arch models fabricated were of a Romanesque geometry (models 1 and 2). This shape is the most common aortic arch geometry throughout the global population (80%) and resembles a normal rounded aortic arch compared to the less common angular Gothic (model 4) and the crenel (model 3) shapes. Three types of aortic arch geometries have been described by Demertzis et al. [31]. The aortic arch types of I, II, or III use the vertical distance from the origin of the BCT to the top of the arch in the parasagittal "stretched-out" criterion. If this distance is <1 diameter of the LCCA, the arch is a type I arch (model 2), between 1 and 2 diameters in a type II arch (models 1 and 3), and >2 diameters in a type III arch (model 4) [43]. Model 3 was the only arch displaying a variation in branching patterns (bovine arch). There are nine reported variations in branching patterns [28].

720 bovine embolus analogs were released from three different positions and tracked through four patient-specific models under three flow conditions. The EAs were fabricated from stagnated mammalian blood. Chueh et al. [25] utilized thrombin-induced bovine emboli to mimic fresh red clots commonly found in patients with stroke, which would be the gold standard clot analog for such embolization investigations. Such biological emboli are superior to the lobster hemolymph [24], acrylic synthetics [19], and the micro particles [22,23] used in previous in vitro systems. The motivation related to the selection of the emboli's size was inspired by patient-specific cases. Middle cerebral artery (MCA) occlusion is the most common site for cardioembolic strokes [44]. The MCA measures a diameter of 3–4 mm and so would indicate a lodging embolus of similar diameter size. Thambidorai et al. [42] describe the size of atrial and atrial appendage emboli of 0.2–4.2 cm and 1.0–3.9 cm in width with an area of 0.1–8.0 cm^2 and 0.9–7.0 cm^2, respectively. Menke et al. [10] also describe clots associated with the left atrium ranging in size from a few millimeters to 4 cm. Clark et al. [26] and Chueh et al. (2014) fabricated synthetic and mammalian clot analogs, respectively, all

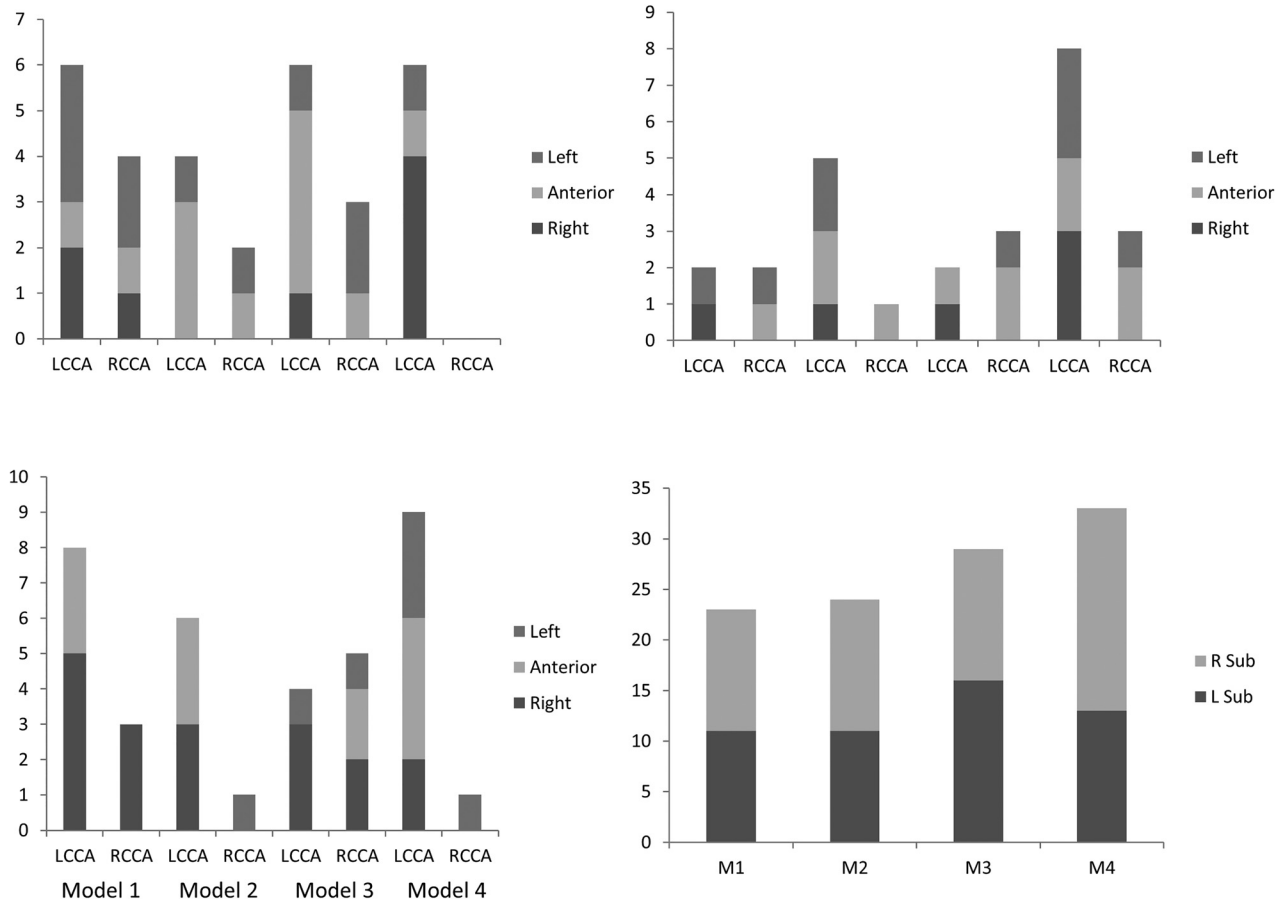

Fig. 8 Bar chart of the variation in the number of clots traveling through the LCCA and RCCA when released from left, anterior, and right entry locations under (*a*) steady flow, (*b*) normal flow, (*c*) AF flow, and (*d*) bar chart of the overall number of clots that traveled through the left and right subclavian arteries

within this range. Most computational work reported the use of idealized particles [16–18] and microparticles [10,13,14], which are useful but not representative of clots retrieved from patient cases. They also do not capture the behavior of a clot under physiological flow. Fahy et al. [24] reported clots compressing to diameters in vitro resulting in a compaction ratio of 1.1:1 and 4:1.

The clots used in this study were therefore physiologically representative of clots retrieved from stroke patients. The clots were smaller in diameter compared to the diameters of the aortic arch branching vessels, but similar in size to the MCA, a likely location for clot lodgment. The smaller sizes of the clots would lead one to believe more trajectory paths would occur through these vessels. However, clot diameter proved not to as big a defining characteristic in trajectory path as previously thought. Of the clots that successfully passed through the LCCA and RCCA, one clot was over 6 mm in diameter and clots as small as 2 mm in diameter failed to enter the branching vessel and instead traveled through the descending aorta. This could be related with the percentage outlet flowrates and that flowrate through the descending aorta was too powerful for the smaller clots to enter the branching aortic arch vessels. It would be interesting to repeat the experiments with larger diameter clots to investigate clot size and trajectory paths further.

In total, 205 (28.5%) EAs traveled into one of the branching vessels, with 87 (12%), 66 (9%), and 52 (7%) traveling through the BCT, the LCCA, and the L Sub, respectively. Statistically more clots traveled through the BCT, χ^2 (2, $N = 720$) = 12.70, $p < 0.05$. This is possibly due to the fact that the BCT is the first branching vessel available to the embolus to travel through. It is also located parallel to the flow meaning the clot does not have to turn through the aortic arch. There was no statistical difference in the distribution of clot trajectories when the clot was released from the right, left, or anterior positions under steady flow, χ^2 (3, $N = 240$) = 2.30, $p > 0.05$, normal pulsatile flow, χ^2 (3, $N = 240$) = 8.51, $p > 0.05$, and AF pulsatile flow, χ^2 (3, $N = 240$) = 4.33, $p > 0.05$. This is not in agreement with Choi et al. [10] whose simulations demonstrated that clot trajectory was influenced by hemodynamic waveforms and release positions. However, their study included 17 release positions compared to our three release positions. Mukherjee et al. [16] also discussed the strong influence of embolus release instance on embolus distribution to the cerebral vasculature. The ability to control the release position of a clot experimentally is extremely difficult and is a limitation to this study.

In terms of flowrate and embolus trajectory, Chung et al. [23] showed that the distribution of smaller emboli approaches that of the flow, while larger diameter emboli travel along the vessel with the greatest flowrates. Bushi et al. [22] studied emboli trajectory patterns through Y-shaped bifurcation models and showed large spherical particles, of diameters 0.6, 1.6, and 3.2 mm, preferentially entering the wider bifurcation branch. Our results show that the number of clots traveling through the varying branches was proportional to the flowrate. Our results showed that 25–35% of EAs traveled along the branching vessels for all tests. This percentage of EAs was proportional to the percentage flowrate split of 25–31% along the branching vessels. AF accounts for approximately 45% of cardiogenic strokes. Many cryptogenic strokes are classified as cardiogenic, but only one third of these patients exhibit AF symptoms [45]. Our results show that of the 63 EAs that traveled through the LCCA and RCCA under pulsatile flow

conditions, 41% traveled through the common carotid arteries in the absence of AF. A link can so be drawn that not only does AF contribute to the formation of clots, but it can also be shown to alter the hemodynamics to increase the chances of a clot to travel through the branching vessels of the aortic arch.

Under steady flow, models 1 and 3 had more CCA trajectories (10 EAs each) than models 2 and 4 (6 EAs each). Models 1 and 3 displayed larger RCCA and LCCA vessel diameters than models 2 and 4, which may account for the rise in number of trajectories. Clark et al. (2015) released 300 spherical particles simulating thrombi under a steady-state continuous flow loop in an idealized Romanesque aortic arch phantom model to validate numerical data [26]. Steady flow testing allows for a level of reproducibility between models and allows for an uninterrupted testing mechanism as the EA can be inserted while the fluid is flowing. However, it cannot be inferred equivalent between models for physiological similarity [26]. It must also be noted that model 3 was the only model to experience a trajectory through the vertebral artery. This was not seen in any other model under any other flow condition. Strokes occurring in the VAs are not common among stroke patients, with the most likely etiology being small vessel occlusion and not cardiogenic embolism [44].

Under healthy/normal pulsatile flow conditions, model 4 had the greatest number of CCA trajectories (11 EAs) compared to models 1–3 (4 EAs, 6 EAs, and 5 EAs, respectively). This was in agreement with numerical simulations of EA trajectories [13] and is attributed to the positioning of the branching vessels in relation to the aortic arch. Model 4 is a type III arch and the branching vessels (brachiocephalic trunk, LCCA, and left subclavian artery) are parallel to the inlet flow stream and thus could result in more EAs traveling through these vessels. Branching among the other three models is located higher along the aortic arch. It is also noted that under normal pulsatile flow, model 3 is the only arch displaying a variation in branching patterns (bovine arch) and could account for the reduced number of clots traveling toward the peripherals (15%) compared to models 2 and 4 (both 20%)

AF and steady flow displayed similar CCA trajectory counts for models 1–3. This could be due to the fact that the short cardiac cycle length was not too dissimilar to a nonstop, steady flow. Overall, AF flow conditions increased trajectories through the LCCA and RCCA by 25% when compared to normal flow. This increase in clot trajectories under AF flow conditions was also shown by Choi et al. [10], who computationally simulated the ejection of dimensionally similar clots (diameter = 2–6 mm). The reduction in cardiac output and cycle length may have a more significant impact on clot trajectory patterns and therefore embolic stroke than previously thought. The shorter cardiac output cycle length associated with AF results in shorter distances traveled by the EAs after each beat. The EAs then have a greater chance of re-routing and traveling toward the extra-cranial vasculature. Mukheree et al. (2016) discussed that particle interaction with helical flow could be a crucial factor in the transport of emboli. A further study to visualize the effects of AF on flow helicity could better explain this change in stroke propensity [17].

Choi et al. [13] demonstrated that curvature pattern and angulation of aortic arches can play a determinant role in AF-induced stroke propensity. They showed that arches of lower curvature angle, like that seen in Romanesque, and crenel arches experienced an increase in EA trajectories through the branching vessels under AF flow conditions. The same was not seen in our results. The variation in arch shape and type of our 4 models was not statistically significant in clot trajectory patterns under χ^2 statistics ($p > 0.05$). However, there was an obvious variation in clot trajectory and model shape, with model 4 having the most CCA trajectories (27 clots). Model 4 was a type III arch and all the branching vessels were parallel to the inlet flow stream contributing to more EAs traveling through these vessels. Including a greater sample size of arches in future studies, with varying branching patterns could investigate the role geometry plays in aortic hemodynamics and clot trajectories in much more detail.

Choi et al. [10] also showed computationally that the difference in the number of clots traveling through the LCCA to be about 60% between the normal and AF flow conditions. This was in agreement with our findings (59%). There are conflicting arguments in the literature regarding left–right propensity of cardiogenic emboli. Cardiogenic emboli are known to have right brain propensity owning to the fact that the RCCA branches first from the aortic arch [18,46–48]. Gold et al. [47] investigated the role of arch geometry in right–left brain propensity. Although there was a slight trend in right side infarcts in a standard arch, this was not statistically significant. Other clinical reports suggest left hemisphere strokes are more common than right hemisphere strokes as ischemic strokes are more frequent in the left MCA as a result of cardioembolism [49,50]. These studies propose vessel thickness and geometry as the reason for LCCA propensity among cardiogenic emboli.

The recorded outlet flowrates through the model LCCA and RCCAs were kept equal and therefore the tendency for EAs to travel through the LCCA or RCCA could be attributed to aortic arch branching and location. The BCT did experience the most trajectories probably because it branches first from the aortic arch; however, the split between the right subclavian and RCCA resulted in a majority of trajectories traveling through the right subclavian compared to the RCCA. This could explain the drop in count for RCCA trajectories compared to LCCA trajectories. Our sample size of arches was small ($n = 4$) compared to clinical studies with hundreds of patients and therefore a greater sample size and variation in arches could investigate this propensity further. Aortic arch models with different branching vessels and configurations should be included in future studies to fully understand this conflicting argument between RCCA and LCCA propensity in stroke occurrence.

Models 1–3 were derived from computed tomography scans of stroke patients where emboli blockages occurred on the right side. Model 1 was derived from a patient who suffered a blocked M1 right, which would indicate a blood clot trajectory through the RCCA. From the data in our study, there was an equal chance that the clot would travel through either LCCA or RCCA under normal pulsatile flow conditions. However, under AF conditions, this shifts in favor of the LCCA:RCCA (72:27%). Model 2 was derived from a patient who experienced blockage of the M1 right blood vessel and there was a 1.6% chance of this occurring under AF flow conditions. Model 3 was from a patient with a Crenel aortic arch and a blockage of the distal ICA right vessel and exhibited a greater chance of EAs traveling through the RCCA under both healthy and AF flow conditions. From this, it can be seen that AF was fundamental in the trajectory patterns of those patient clots.

The results also highlight the emboli trajectory distribution toward the left and right subclavian arteries and the descending aorta. The majority of EAs released into our system traveled along these vessels, which correlates with previous work [16]. Knowledge of embolus transport to other vascular regions can aid in disease diagnosis and examining etiological factors of embolic occlusive disorders such as renal artery occlusion and acute limb ischemia [16]. Two percent of patients with cardiogenic brain embolism have clinically recognized peripheral emboli. While necropsy studies of patients with brain embolism note that infarcts are often found in the spleen, kidneys, and other organs, the symptoms of peripheral embolism are typically very minor and nonspecific (e.g., transient abdominal discomfort, and leg cramp) that they are rarely diagnosed correctly [12].

5 Limitations

The present study has several limitations. First, it must be noted that sourcing suitable computed tomography scans that capture the entire aortic arch, with ascending/descending aorta and branching vessels, is very difficult. Sourcing such datasets, such as the ones presented here from AF stroke patient cases, is also very challenging. The Romanesque aortic arch shape, being the

most common among the world's population, is the most commonly seen among image datasets. We were fortunate enough to have one crenel and one gothic aortic arch among our repository of aortic arch sets and these too were chosen for manufacture to test the hypothesis that aortic arch geometry influences clot trajectory. Models 1, 2, and 4 all display the normal three-branch pattern and model 3 displayed a bovine arch branching pattern. However, two-branch and four-branch patterns are also potential branching patterns found in patients. It is well known that aortic hemodynamics display large variability as a result of arch and branching variation. This study only used four cases of aortic arch and although difficult to obtain, a greater number of datasets with aortic arch variation could provide more statistical significance with regard to the effect arch geometry has on emboli trajectories.

Second, it should be highlighted that the term patient-specific refers to the aortic arch and shape of the patient vasculature, but not the flow conditions. Although the normal and AF flow profiles are considered representative of biological flow conditions in this study, it must be mentioned that the patient-specific outlet flow splits were unknown. The pressure at the outlet boundaries was also not measured and a Windkessel model to influence downstream impedance was not used. The rigidity of the models was also a limitation to the study. Future work should include more flexible model cases and patient physiological data such as outlet flow and blood pressure data, if possible, to create a true patient-specific investigation.

Chueh et al. [25] utilized thrombin induced bovine emboli to mimic fresh red clots commonly found in patients with stroke, which would be the gold standard clot analog for such embolization investigations. Releasing varying EAs such as Chueh et al. [25] and other EAs described in literature would give a broader analysis of emboli trajectory paths. Increasing the number of release positions would further improve the investigation into the relationship between aortic arch hemodynamics and emboli trajectory patterns. Automation of the release mechanism in this physiological simulation system would be beneficial in controlling the injection of the EAs and a camera of greater frame rate and pixilation could improve the ability to monitor clot trajectory more closely. The use of other apparatus such as particle image velocimetry could also improve the measurement of the flow split at the outlet boundary conditions and help understand the LCCA versus RCCA propensity problem.

Embolization as a result of AF was not fully simulated in this work. Embolization is comprised of two components, formation and transport. During AF, blood is not pumped completely out of the heart when the heart beats, allowing some blood to pool in the left atrium and/or the left atrial appendage. Stagnant blood coagulates and increases thrombin and platelet activation, creating a thrombus. Coagulation time can differ from the composition of the thrombus prior to embolization. The static method of inducing coagulation in mammalian blood using thrombin was used in this study [51]. This method has been utilized successfully in previous studies that analyze the mechanical properties of EAs [40,41]. The Chandler loop method [52] is another technique used to manufacture viable EAs. It has been shown that EAs produced using the Chandler loop method have more biochemical similarity to those formed in vivo [53]. However, as the main objective of this study was to analyze EA trajectory patterns under physiological flow conditions, the static method proved sufficient to create the quantity of EAs required for testing. To fully replicate the physiological process of AF, a system should be devised wherein a blood clot is created and emitted into a closed-loop flow system.

Finally, patients with AF can often have other factors associated with stroke risk and occurrence such as heart disease, age, duration of arrhythmia, chronic vs intermittent fibrillation, and atrial size [54]. Therefore, the presence of a possible cardiac source of embolism does not necessarily mean that the stroke was caused by a cardiogenic embolism. Coexisting atherosclerotic cerebrovascular disease is also a common cause of stroke in such patients. Further studies are required to understand the full relationship between AF and the aortic arch and cardioembolic trajectories, which could lead to a more comprehensive stroke prevention treatment for patients with AF.

6 Conclusion

Despite the limitations in this study, it is evident that the EA trajectory paths were proportional to the percentage flowrate split of 25–31% along the branching vessels. AF flow conditions increased the number of EA trajectories to the head, with left-sided propensity. There was no statistical difference in the distribution of clot trajectories when the clot was released from the right, left, or anterior positions. A great proportion of EAs traveled peripherally though the right and left subclavian blood vessels and down the descending aorta. Further studies should be employed to understand the role that these clots would play on patient health and further disease under various physiological flow conditions.

Acknowledgment

Abattoir: Burkes, Gort, Galway.

References

[1] Lakhan, S. E., Kirchgessner, A., and Hofer, M., 2009, "Inflammatory Mechanisms in Ischemic Stroke: Therapeutic Approaches," J. Transl. Med., **7**, p. 97.
[2] Kannel, W. B., and Benjamin, E. J., 2008, "Status of the Epidemiology of Atrial Fibrillation," Med. Clin. North Am., **92**(1), pp. 17–40.
[3] Kelley, R. E., and Alireza, M., 2003, "Cardioembolic Stroke: An Update," South. Med. J., **96**(4), p. 343.
[4] Beldi, G., Beng, L., Siegel, G., Bisch-Knaden, S., and Candinas, D., 2007, "Prevention of Perioperative Thromboembolism in Patients With Atrial Fibrillation," Br. J. Surg., **94**(11), pp. 1351–1355.
[5] Blackshear, J. L., and Odell, J. A., 1996, "Appendage Obliteration to Reduce Stroke in Cardiac Surgical Patients With Atrial Fibrillation," Ann. Thorac. Surg., **61**(2), pp. 755–759.
[6] Menke, J., Lüthje, L., Kastrup, A., and Larsen, J., 2010, "Thromboembolism in Atrial Fibrillation," Am. J. Cardiol., **105**(4), pp. 502–510.
[7] Fuster, V., Ryden, L. E., Cannom, D. S., Crijns, H. J., Curtis, A. B., Ellenbogen, K. A., Halperin, J. L., Le Heuzey, J. Y., Kay, G. N., Lowe, J. E., Olsson, S. B., Prystowsky, E. N., Tamargo, J. L., Wann, S., Smith, S. C., Jr., Jacobs, A. K., Adams, C. D., Anderson, J. L., Antman, E. M., Halperin, J. L., Hunt, S. A., Nishimura, R., Ornato, J. P., Page, R. L., Riegel, B., Priori, S. G., Blanc, J. J., Budaj, A., Camm, A. J., Dean, V., Deckers, J. W., Despres, C., Dickstein, K., Lekakis, J., McGregor, K., Metra, M., Morais, J., Osterspey, A., Tamargo, J. L., and Zamorano, J. L., 2006, "Guidelines for the Management of Patients With Atrial Fibrillation," Circulation, **114**(7), pp. 257–354.
[8] Heeringa, J., van der Kuip, D. A., Hofman, A., Kors, J. A., van Herpen, G., Stricker, B. H., Stijnen, T., Lip, G. Y., and Witteman, J. C., 2006, "Prevalence, Incidence and Lifetime Risk of Atrial Fibrillation: The Rotterdam Study," Eur. Heart J., **27**(8), pp. 949–953.
[9] Prystowsky, E. N., 2008, "The History of Atrial Fibrillation: The Last 100 Years," J. Cardiovasc. Electrophysiol., **19**(6), pp. 575–582.
[10] Choi, H. W., Navia, J. A., and Kassab, G. S., 2013, "Stroke Propensity Is Increased Under Atrial Fibrillation Hemodynamics: A Simulation Study," PLoS One, **8**(9), p. e78435.
[11] Khodaee, F., Vahidi, B., and Fatouraee, N., 2016, "Analysis of Mechanical Parameters on the Thromboembolism Using a Patient-Specific Computational Model," Biomech. Model Machanobiol., **15**(5), pp. 1295–1305.
[12] Osorio, A. F., Osorio, R., Ceballos, A., Tran, R., Clark, W., Divo, E. A., Argueta-Morales, I. R., Kassab, A. J., and DeCampli, W. M., 2013, "Computational Fluid Dynamics Analysis of Surgical Adjustment of Left Ventricular Assist Device Implantation to Minimize Stroke Risk," Comput. Methods Biomech. Biomed. Eng., **16**(6), pp. 622–632.
[13] Choi, H. W., Lou, T., Navia, J. A., and Kassab, G. S., 2017, "Role of Aortic Geometry on Stroke Propensity Based on Simulations of Patients Specific Models," Sci. Rep., **7**, p. 7065.
[14] Fabbri, D., Long, Q., Das, S., and Pinelli, M., 2014, "Computational Modelling of Emboli Travel Trajectories in Cerebral Arteries: Influence of Microembolic Particle Size and Density," Biomech. Model. Mechanobiol., **13**(2), pp. 289–302.
[15] Shadden, S. C., and Arzani, A., 2015, "Lagrangian Postprocessing of Computational Hemodynamics," Ann. Biomed. Eng., **43**(1), pp. 41–58.
[16] Mukherjee, D., and Shadden, S. C., 2017, "Inertial Particle Dynamics in Large Artery Flows–Implications for Modeling Arterial Embolisms," J. Biomech., **52**, pp. 155–164.
[17] Mukherjee, D., Padilla, J., and Shadden, S. C., 2016, "Numerical Investigation of Fluid–Particle Interactions for Embolic Stroke," Theor. Comput. Fluid Dyn., **30**(1–2), pp. 23–39.

[18] Mukherjee, D., Jani, N. D., Selvaganesan, K., Weng, C. L., and Shadden, S. C., 2016, "Computational Assessment of the Relation Between Embolism Source and Embolus Distribution to the Circle of Willis for Improved Understanding of Stroke Etiology," ASME J. Biomech. Eng., **138**(8), p. 081008.
[19] Aycock, K. I., Campbell, R. L., Manning, K. B., and Craven, B. A., 2017, "A Resolved Two-Way Coupled CFD/6-DOF Approach for Predicting Embolus Transport and the Embolus-Trapping Efficiency of IVC Filters," Biomech. Model. Mechanobiol., **16**(3), pp. 851–869.
[20] Conti, M., Vandenberghe, S., Marconi, S., Ferrari, E., Romarowski, R. M., Morganti, S., Auricchio, F., and Demertzis, S., 2018, "Reversed Auxiliary Flow to Reduce Embolism Risk During TAVI: A Computational Simulation and Experimental Study," Cardiovasc. Eng. Technol., **10**(1), pp. 124–135.
[21] Mukherjee, D., Jani, N. D., Narvid, J., and Shadden, S. C., 2018, "The Role of Circle of Willis Anatomy Variations in Cardio-Embolic Stroke: A Patient-Specific Simulation Based Study," Ann. Biomed. Eng., **46**(8), pp. 1128–1145.
[22] Bushi, D., Grad, Y., Einav, S., Yodfat, O., Nishri, B., and Tanne, D., 2005, "Hemodynamic Evaluation of Embolic Trajectory in an Arterial Bifurcation," Stroke, **36**(12), pp. 2696–2700.
[23] Chung, E. M. L., Hague, J. P., Chanrion, M.-A., Ramnarine, K. V., Katsogridakis, E., and Evans, D. H., 2010, "Embolus Trajectory Through a Physical Replica of the Major Cerebral Arteries," Stroke, **41**(4), pp. 647–652.
[24] Fahy, P., Malone, F., McCarthy, E., McCarthy, P., Thornton, J., Brennan, P., O'Hare, A., Looby, S., Sultan, S., Hynes, N., and Morris, L., 2015, "An In Vitro Evaluation of Emboli Trajectories Within a Three-Dimensional Physical Model of the Circle of Willis Under Cerebral Blood Flow Conditions," Ann. Biomed. Eng., **43**(9), pp. 2265–2278.
[25] Chueh, J. Y., Puri, A. S., Wakhloo, A. K., and Gounis, M. J., 2014, "Risk of Distal Embolization With Stent Retriever Thrombectomy and ADAPT," J. Neurointervent Surg, **8**(2), pp. 197–202.
[26] Clark, W. D., Eslahpazir, B. A., Argueta-Morales, I. R., Kassab, A. J., Divo, E. A., and DeCampli, W. M., 2015, "Comparison Between Bench-Top and Computational Modelling of Cerebral Thromboembolism in Ventricular Assist Device Circulation," Cardiovasc. Eng. Technol., **6**(3), pp. 242–255.
[27] Pollanen, M. S., 1991, "Behavior of Suspended Particles at Bifurcations: Implications for Embolism," Phys. Med. Biol., **36**(3), pp. 397–401.
[28] Uflacker, R., 2007, *Atlas of Vascular Anatomy: An Angiographic Approach*, Lippincott Williams & Wilkins, Charleston, SC, pp. 133–163.
[29] Ou, P., Celermajer, D. S., Mousseaux, E., Giron, A., Aggoun, Y., Szezepanski, I., Sidi, D., and Bonnet, D., 2007, "Vascular Remodeling After 'Successful' Repair of Coarctation Impact of Aortic Arch Geometry," J. Am. Coll. Cardiol., **49**(8), pp. 883–890.
[30] Agnoletti, G., Ou, P., Celermajer, D. S., Boudjemline, Y., Marini, D., Bonnet, D., and Aggoun, Y., 2008, "Acute Angulation of the Aortic Arch Predisposes a Patient to Ascending Aortic Dilatation and Aortic Regurgitation Late After the Arterial Switch Operation for Transposition of the Great Arteries," J. Thorac. Cardiovasc. Surg., **135**(3), pp. 568–572.
[31] Demertzis, S.,Hurni, S., Stalder, M., Gahl, B., Herrmann, G., and Van den Berg, J., 2010, "Aortic Arch Morphometry in Living Humans," J. Anat., **217**(5), pp. 588–596.
[32] Reymond, P., Merenda, F., Perren, F., Ruefenacht, D., and Stergiopulos, N., 2009, "Validation of a One-Dimensional Model of the Systemic Arterial Tree," Am. Physiol. Soc., **297**(1), pp. 208–222.
[33] Clark, D. M., Plumb, V. J., Epstein, A. E., and Kay, G. N., 1997, "Hemodynamic Effects of an Irregular Sequence of Ventricular Cycle Lengths During Atrial Fibrillation," J. Am. Coll. Cardiol., **30**(4), pp. 1039–1045.
[34] Stein, P. D., and Sabbah, H. N., 1976, "Turbulent Blood Flow in the Ascending Aorta of Humans With Normal and Diseased Aortic Valves," Circ. Res., **39**(1), pp. 58–65.
[35] Hennen, B., Markwirth, T., Scheller, B., Schäfers, H. J., and Wendler, O., 2001, "Do Changes in Blood Flow in the Subclavian Artery Affect Flow Volume in IMA Grafts After Complete Arterial Revascularization With the T-Graft Technique?," Thorac. Cardiovasc. Surg., **49**(2), pp. 84–88.
[36] Tokuda, Y., Song, M. H., Ueda, Y., Usui, A., Akita, T., Yoneyama, S., and Maruyama, S., 2008, "Three-Dimensional Numerical Simulation of Blood Flow in the Aortic Arch During Cardiopulmonary Bypass," Eur. J. Cardio-Thorac. Surg., **33**(2), pp. 164–167.
[37] Sato, K., Ogoh, S., Hirasawa, A., Oue, A., and Sadamoto, T., 2011, "The Distribution of Blood Flow in the Carotid and Vertebral Arteries During Dynamic Exercise in Humans," J. Physiol., **589**(11), pp. 2847–2856.
[38] Benim, A. C., Nahavandi, A., Assmann, A., Schubert, D., Feindt, P., and Suh, S. H., 2011, "Simulation of Blood Flow in Human Aorta With Emphasis on Outlet Boundary Conditions," Appl. Math. Modell., **35**(7), pp. 3175–3188.
[39] Bürk, J., Blanke, P., Stankovic, Z., Barker, A., Russe, M., Geiger, J., Frydrychowicz, A., Langer, M., and Markl, M., 2012, "Evaluation of 3D Blood Flow Patterns and Wall Shear Stress in the Normal and Dilated Thoracic Aorta Using Flow Sensitive 4D CMR," J. Cardiovasc. Magn. Reson., **14**, p. 84.
[40] Malone, F., MacCarthy, E., Delassus, P., Fahy, P., Kennedy, J., Fagan, A. J., and Morris, L., 2018, "The Mechanical Characterisation of Bovine Embolus Analogues Under Various Loading Conditions," Cardiovasc. Eng. Technol., **9**(3), pp. 489–502.
[41] Chueh, J. K., Wakhloo, A. K., Hendricks, G. H., Silva, C. F., Weaver, J. P., and Gounis, M. J., 2011, "Mechanical Characterisation of Thromboemboli in Acute Ischemic Stroke and Laboratory Embolus Analogs," Am. J. Neurobiol., **32**(7), pp. 1237–1244.
[42] Thambidorai, S. K., Murray, R. D., Parakh, K., Shah, T. K., Black, I. W., Jasper, S. E., Li, J., Apperson-Hansen, C., Asher, C. R., Grimm, R. A., and Klein, A. L., 2005, "Utility of Transesophageal Echocardiography in Identification of Thrombogenic Milieu in Patients With Atrial Fibrillation (An ACUTE Ancillary Study)," Am. J. Cardiol., **96**(7), pp. 935–941.
[43] Madhwal, S., Rajagopal, V., Bhatt, D. L., Bajzer, C. T., Whitlow, P., and Kapadia, S. R., 2008, "Predictors of Difficult Carotid Stenting as Determined by Aortic Arch Angiography," J. Invasive Cardiol, **20**(5), pp. 200–204.
[44] Chung, J. W., Park, S. H., and Kim, N., 2014, "Trial of ORG 10172 in Acute Stroke Treatment (TOAST) Classification and Vascular Territory of Ischemic Stroke Lesions Diagnosed by Diffusion-Weighted Imaging," J. Am. Heart Assoc., **3**(4), p. e001119.
[45] Sanna, T., Diener, H.-C., Passman, R. S., Di Lazzaro, V., Bernstein, R. A., Morillo, C. A., Rymer, M. M., Thijs, V., Rogers, T., Beckers, F., Lindborg, K., Brachmann, J., and CRYSTAL AF Investigators, 2014, "Cryptogenic Stroke and Underlying Atrial Fibrillation," N. Engl. J. Med., **370**(26), pp. 2478–2486.
[46] Park, K. Y., Kim, Y. B., Chung, P. W., Moon, H. S., Suh, B. C., Yoon, K. J., and Lee, Y. T., 2014, "Right Side Propensity of Cardiogenic Emboli in Acute Ischemic Stroke With Atrial Fibrillation," Scand. Cardiovasc. J., **48**(6), pp. 335–338.
[47] Gold, M., Khamesi, M., Sivakuma, M., Natarajan, V., Motahari, H., and Caputo, N., 2018, "Right-Left Propensity of Cardiogenic Cerebral Embolism in Standard Versus Bovine Aortic Arch Variant," Clin. Anat., **31**(3), pp. 310–313.
[48] Meyer, J. S., Charney, J. Z., Rivera, V. M., and Mathew, M. T., 1971, "Cerebral Embolization: Prospective Clinical Analysis of 42 Cases," Stroke, **2**(6), pp. 541–554.
[49] Hedna, W. S., Bodhit, A. N., Ansari, S., Falchook, A. D., Stead, L., Heilman, K. M., and Waters, M. F., 2013, "Hemispheric Differences in Ischemic Stroke: Is Left Hemisphere Stroke More Common?," J. Clin. Neurol., **9**(2), pp. 97–102.
[50] Rodriguez Hernandez, S., Kroon, A. A., van boztel, M. P. J., Mess, W. H., Lodder, J., Jolles, J., and de leeuw, P. W., 2003, "Is There Side Predilection for Cerebrovascular Disease?," Hypertension, **42**(1), pp. 56–60.
[51] Gralla, J., Schroth, G., Remonda, L., Fleischmann, A., Fandino, J., Slotboom, J., and Brekenfeld, C., 2006, "A Dedicated Animal Model for Mechanical Thrombectomy in Acute Stroke," AJNR, **27**(6), pp. 1357–1361.
[52] Chandler, A. B., 1958, "In Vitro Thrombotic Coagulation of the Blood; a Method for Producing a Thrombus," Lab Invest., **7**(2), pp. 110–114.
[53] Mutch, N. J., Moore, N. R., Mattsson, C., Jonasson, H., Green, A. R., and Booth, N. A., 2008, "The Use of the Chandler Loop to Examine the Interaction Potential of NXY—059 on the Thrombolytic Properties of rtPA on Human Thrombi In Vitro," Br. J. Pharmacol., **153**(1), pp. 124–131.
[54] Leary, M. C., and Caplan, L. R., 2008, "Cardioembolic Stroke: An Update on Etiology, Diagnosis and Management," Ann. Indian Acad. Neurol., **11**(5), pp. 52–63.